Proceedings of the ASME 2024
Conference on Fluid Power and Motion Control
FPMC2024
September 11-13, 2024, Bath, UK

FPMC2024-140393

A COMPACT ELECTROPERMANENT MAGNET VALVE GEOMETRY FOR SWITCHING OF MAGNETORHEOLOGICAL FLUID USING PARTICLE JAMMING

James Gallentine[1](james.c.gallentine@vanderbilt.edu), Nithin S. Kumar [1](nithin.s.kumar@vanderbilt.edu), Eric J. Barth,[1](eric.j.barth@vanderbilt.edu)

[1]Vanderbilt University, Nashville, TN

ABSTRACT

Electropermanent magnetic (EPM) valves consist of two permanent magnets, one with high coercivity and one with relatively low coercivity, which are able to rapidly redirect the flux within a magnetic circuit. When combined with magnetorheological (MR) fluid, they provide the ability to rapidly switch flow in a hydraulic circuit on or off. EPM valves contain no moving parts and draw no power except when changing state. These facts, along with their scalability, make them an attractive option for distributed flow control in small hydraulic systems. Current examples of EPM valves are often restricted to relatively low-pressure or low-flow operation. Miniaturization of small-scale hydraulic robots, both soft and rigid, is limited by the availability of sufficiently lightweight, compact, and efficient components which are capable of directing fluid at pressures greater than 700 kPa. This research proposes an EPM valve which leverages the magnetic properties of MR fluid to channel magnetic flux through the fluid.

To evaluate the proposed geometry, an exploratory prototype was constructed and evaluated using a test-bench capable of evaluating the valve as a flow resistance. Simulations were conducted to evaluate the design and validate the use of simulation for future design iteration.

To be of use in robotic systems, this valve needs to be capable of rapidly switching relatively high pressures while maintaining a highly compact and easily manufactured form factor. Due to its size and low power consumption, it is suitable for distributed hydraulic control in miniature systems such as hydraulically-actuated robots, including soft robots.

Keywords: Compact Fluid Power, Digital and Proportional Valves, Soft Robotics, Control

1. INTRODUCTION

This work is motivated by the following question: if one wanted to make a practical, highly-dexterous soft robot with hundreds of individually controlled actuators in a compact form, how might such a system look? Nature has several examples of such manipulable forms: octopus arms have been observed to have more than 16,500 arm deformations [1] and elephants have more than 40,000 muscles in their trunks alone. Current state-of-the-art rigid and soft robots are unable to match such dexterity. For example, robots in the media such as Atlas, designed by Boston Dynamics, which leverage the power density of hydraulics, possess only tens of actuated degrees of freedom (Atlas has 28 [2]). Many others rely on a one-motor-per-actuated-degree-of-freedom architecture to provide motion control. There is therefore, a significant gap in the control dexterity exhibited between current robots and biological systems.

Since a soft robot's structure also serves as its actuators, it is possible to build a high number of actuation units within a small structure. Most fluidic soft robots employ an air compressor and a bank of bulky valves external to the robot; this large valve bank limits the number of control channels, in a manner similar to the one-motor-per-actuated-degree-of-freedom architecture of conventional robots: limiting their use for untethered applications or in confined spaces.

The problem remains: how to control this high number of actuators. Electropermanent magnets (EPM), first proposed in [3], are solid-state devices able to rapidly switch between 'on' and 'off' states using a pulse of electric current. They consist of two magnetic materials, one with low (soft magnetic material) and one with high (hard magnetic material) coercivity. The soft magnetic material can be re-magnetized with magnetic poles reversed using a simple solenoid wrapped around the magnet. Once switched, EPMs require no further electrical input to maintain their state. When combined with MR fluid, which hardens under the influence of a magnetic field, EPM valves can enable rapid and efficient switching of fluidic flow [4]. EPM valves have been presented with various alterations to improve their fluidic resistance as shown in [5–7]. Here we present a design with no moving parts which leverages a Neodymium-Iron-Boron (NdFeB) magnet to provide a large magnetic flux density and a grade 5 Aluminum-Nickle-Cobalt (AlNiCo) magnet to enable

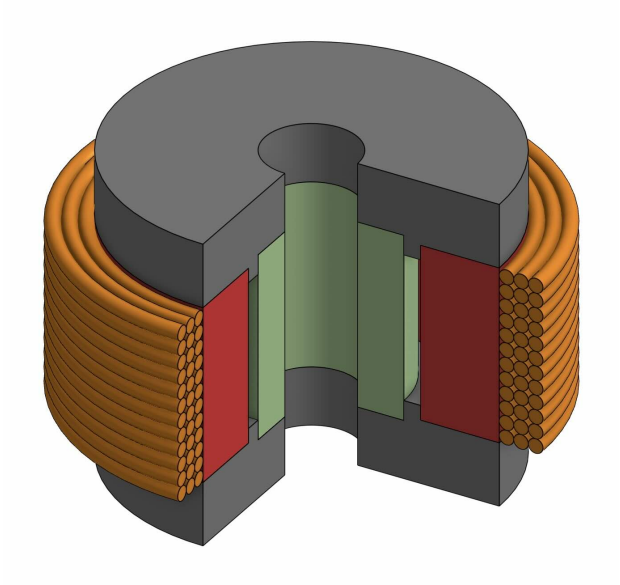

FIGURE 1: THE PROPOSED EPM VALVE ARRANGEMENT WITH CUTAWAY TO SHOW INNER GEOMETRY. GREEN: NDFEB MAGNET. RED: ALNICO MAGNET. GREY: FERROUS END PLATES TO PROVIDE FLUX RETURN. ORANGE: COIL FOR REMAGNETIZING ALNICO MAGNET.

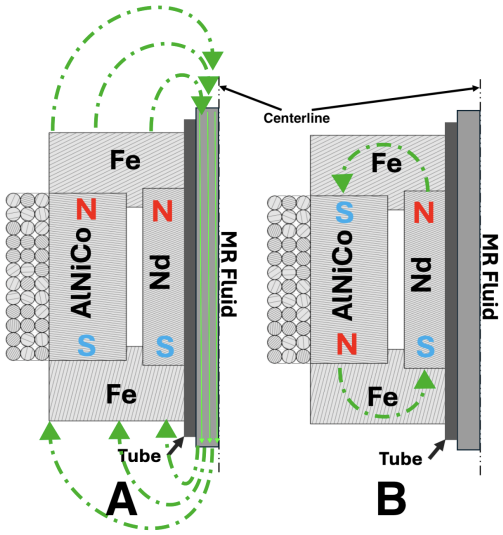

FIGURE 2: EPM VALVE STATES. A: WHEN MAGNETIZED SUCH THAT THE POLES ALIGN, THE EPM VALVE WILL BE IN THE 'CLOSED' STATE AND FLUX WILL BE DIRECTED THROUGH THE MR FLUID. B: WHEN MAGNETIZED SUCH THAT THE POLES ARE OPPOSITE, THE EPM VALVE WILL BE 'OPEN' AND FLUX WILL FLOW PRIMARILY WITHIN THE MAGNETS.

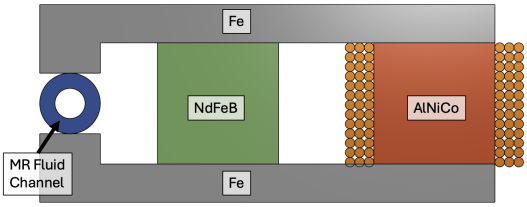

FIGURE 3: ARRANGEMENT OF MAGNETS IN GENERAL EPM VALVES. GREEN: CYLINDRICAL NDFEB MAGNET. RED: CYLINDRICAL ALNICO MAGNET WITH SOLENOID

re-magnetization and flux redirection, rapidly blocking MR fluid flow. In particular, we hypothesize that by employing ring magnets as opposed to standard cylindrical-form magnets typically exhibited in the literature, we will be able to use a relatively larger magnet for a given overall valve size, thereby increasing the magnetic flux available to block fluid flow.

As part of a larger robotic system, we propose a centralized hydraulic supply with miniature, solid-state valves distributed throughout a soft robot akin to the prime mover architecture of heavy machinery. This architecture would feature one centralized prime mover in the form of a high-bandwidth, high-pressure, power-dense pump driven by a brushless DC motor [8].

This paper is organized as follows: Section 2 (Design) presents the architecture of the proposed EPM valve and Section 3 (Initial Simulation) details the use of finite element simulation to study the efficacy of the proposed design. Section 4 (Methods) outlines the fabrication of the 3 EPM geometries, MR fluid, and presents the test setup. Section 5 (Experimental Results) highlights the pressure drop across the valve for each design. Performance evaluation and next steps are considered in Section 6 (Discussion) and Section 7 consists of a design investigation conducted using simulation to identify factors which may influence the performance of the proposed EPM valve geometry.

2. DESIGN

Given that each actuated degree of freedom in the proposed system will require an EPM valve, it is desired to produce valves which are as compact as possible. Ideally, such valves would be small enough (<10 mm) to integrate into existing soft robot manufacturing methods such as 3D printing or casting. The desire for compactness is in direct conflict with the desire to use larger magnets capable of generating stronger magnetic fields to jam the MR fluid and increase the flow resistance.

When the AlNiCo magnet is magnetized such that its poles align with the NdFeB magnet, the unit acts as one larger magnet ('on' state). In this arrangement, the magnetic flux which emanates from the magnet will use the MR fluid as a flux return path, causing the fluid to solidify and turning the valve to a 'closed' configuration as depicted on the left of Figure 2. When the AlNiCo magnet is subsequently re-magnitized such that its poles are opposite those of the NdFeB magnet ('off' state), the magnetic flux will flow around the circuit created by the two magnets rather than through the MR fluid, causing an 'open' valve configuration as depicted on the right side of Figure 2. By changing the arrangement of these two magnets, the coil used for re-magnetizing, and the flow path, we hypothesize that we can achieve a valve package smaller than that seen in the literature for a given magnet size.

Generally, EPMs in literature use two cylindrical magnets which are adjacently located with either one or both of the magnets within a solenoid as shown in Figure 3. The proposed design modifies this standard EPM design. Rather than using two cylindrical magnets, two ring magnets are proposed with one nested

within the other as shown in Figure 1. This layout allows for a larger magnet to be used for a given EPM size by eliminating empty space left by cylindrical magnets. It is hypothesized that the increase in magnetic material will increase the magnetic flux which can enter the MR fluid and produce a valve with higher resistance in the closed state. Additionally, this design positions the EPM solenoid externally, mitigating geometric constraints on its size and strength.

3. INITIAL SIMULATION

To understand the efficacy of the proposed EPM valve design, the system was simulated using a multi-physics finite element solver (COMSOL 5.5). In particular, visualizing the change in the magnetic flux path when the EPM valve is switched on would demonstrate of the virtue of this design. The complexity of simulating this system was reduced by assuming a two-dimensional axis-symmetric setup. This is valid as there is negligible variation in the cross-section of the valve when rotated about it's center-line axis. Figure 4a illustrates the model setup, which is dimensionally consistent with the experiment as described in the Methods section. It consists of the MR fluid, modeled as iron powder with a relative permeability of 6 [9], housed in a PVC tube. The low carbon steel plates were modeled with a relative permeability of 5000. The constitutive B-H curves for the NdFeB and AlNiCo grade 5 magnets were obtained from the COMSOL materials library without any modification.

The "Magnetic Fields" physics interface was used to model this system. Magnetic insulation was prescribed around the air domain surrounding the valve. Three Ampere's Law domains were prescribed in this formulation: one for each magnet and one for the MR fluid. In particular, the remanent flux direction of the AlNiCo magnet was reversed to simulate the valve's open or closed configurations. The closed configuration corresponds to high flux density within the MR fluid tube and is given by the AlNiCo remanent flux direction vector $e = [e_r, e_\phi, e_z]^T = [0, 0, 1]^T$. This is parallel to the magnetization of the NdFeB magnet, resulting in a relatively strong flux density within the MR fluid as shown in Figure 4b. This should produce a flow restriction by causing the iron powder in the MR fluid to align perpendicular to this field. Conversely, reversing the AlNiCo magnetization to $e = [0, 0, -1]^T$, results in a flux return path from the NdFeB to the AlNiCo magnet as shown in Fig. 4c. With a weaker magnetic field within the MR fluid tube, this should provide relatively little flow restriction to the MR fluid. Simulation predicts roughly a 2x increase in the average flux density (0.90 T to 1.72 T) between the open and closed configurations within the MR fluid tube with the dimensions prescribed in the Methods section.

4. METHODS

4.1 Valves

Three EPM geometries were manufactured to test the validity of the proposed architecture.

The first, hereafter referred to as "Valve A", shown on the left of Figure 5, was similar to that designed in [4]. It consisted of a grade 5 AlNiCo magnet measuring 6.4 mm in length and 3.2 mm in diameter (McMaster) along with an N52-grade NdFeB magnet of the same dimensions (McMaster). The AlNiCo magnet was wrapped 75 times in 32 awg enameled wire (McMaster). These magnets were sandwiched between ASTM A36 low-carbon steel face-plates (McMaster) measuring 16 x 9 mm and machined so that the gap between the active surfaces was 3.2 mm, matching the outer-diameter of the tubing used.

The second valve, hereafter referred to as "Valve B", shown in the center of Figure 5, used the same layout, however, two ring magnets were used in place of the cylindrical magnets of the first. The AlNiCo ring magnet (Magnet Kingdom) had a 12.9 mm outer-diameter (OD), a 7.5 mm inner-diameter (ID), and a thickness of 5.9 mm. The NdFeB ring magnet (McMaster) had an OD of 6.4 mm, an ID of 3.2 mm, and measured 6.4 mm in length. Both magnets were glued to low-carbon steel face-plates measuring 19 x 30 mm and machined so that the gap at the ends of the pieces was 3.2 mm. This was to serve as a control for the magnets used in the proposed design.

The final valve, hereafter referred to as "Valve C", an exploratory prototype for the proposed geometry is shown on the right of Figure 5. It was manufactured according to the design in Figure 1. It used identical magnets to that of the second design, however, they were assembled such that they were nested concentrically. A 3.2 mm hole ran the entire length of the valve, extending through the each of the face-plates.

4.2 MR Fluid

MR fluid was made by mixing iron filings sized from $[6, 9]$ microns (Sigma Aldrich) and vegetable oil (Costco) at a ratio of $1.00 : 0.27$ g by mass. This yielded a mixture which is approximately 30% iron by volume. Vegetable oil was chosen both because it was readily available and because most organic oils contain oleic acid [10] which has been shown to reduce sedimentation in MR fluids [11].

4.3 Test Setup

To test each valve, the setup shown in Figure 6 was created to pump MR fluid slowly and at a consistent rate. A 3D printed syringe (PLA, Bambu Lab) was driven via lead screw by a Nema 23 stepper motor (Amazon) and a DM542T digital stepper driver (StepperOnline). The syringe outlet was connected to an SPTW-P10R-G14-VD-M12 pressure transmitter (Festo) by 6 ID x 8 OD mm tubing. Distal from the syringe to the pressure transmitter, the tubing was stepped down to a 40 mm length of 1.6 ID x 3.2 OD mm tubing where the EPM valves would be mounted. After the valve, the tubing was stepped back up and a second measured the outlet pressure. Finally, this was fed into a reservoir. The entire setup was mounted vertically to enable the purging of bubbles in the lines and syringe. The test setup was controlled and data collected using Simulink Desktop Real-Time (Mathworks) and an MF634 digital acquisition card (Humusoft).

The EPM valve solenoids were driven using an H-bridge motor driver (Cytron) to allow for reversing the current in the solenoid to turn the EPM on or off. Each valve was powered by a 30 V, 3 A benchtop power supply (Protek).

All tests were conducted at a constant flow-rate of 0.625 [mL/s]. At this flow-rate, the inertial effects of MR fluid on the valve could be ignored. Motor steps were counted to produce an accurate determination of liquid volume flowed.

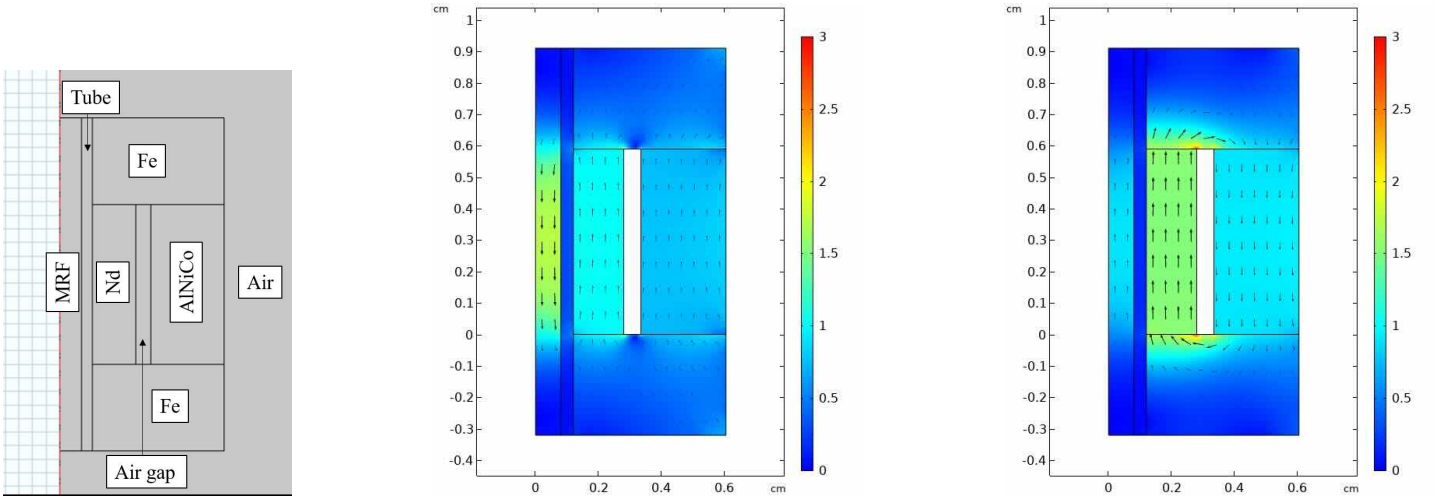

(a) Model setup

(b) EPM valve in the "Closed" state

(c) EPM valve in the "Open" state

FIGURE 4: COMSOL SIMULATION OF THE PROPOSED EPM VALVE. (A) SETUP INCLUDING THE FLUID FLOW CHANNEL CONTAINING MR FLUID LABELED AS 'MRF', (B) MAGNETIC FLUX DENSITY OF THE VALVE IN THE CLOSED STATE, (C) VALVE IN THE 'OPEN' STATE. ARROWS INDICATE THE DIRECTION OF THE MAGNETIC FLUX. COLOR SCALE IN UNITS OF TESLA.

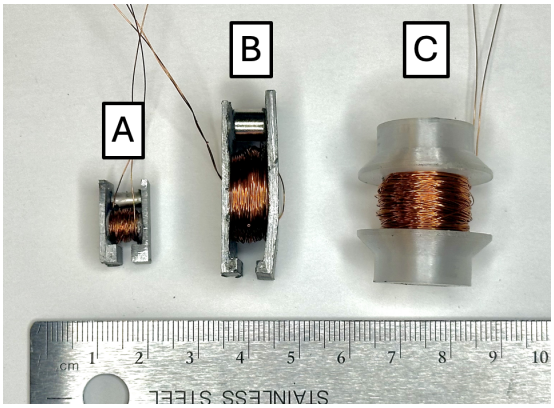

FIGURE 5: THE THREE EPM VALVES PRODUCED. (A) VALVE SIMILAR TO THAT PRESENTED IN [4]. (B) SAME LAYOUT AS (A), BUT WITH IDENTICAL MAGNETS AS USED IN (C). (C) THE PROPOSED DESIGN USING TWO AXIALLY-COINCIDENT RING-MAGNETS.

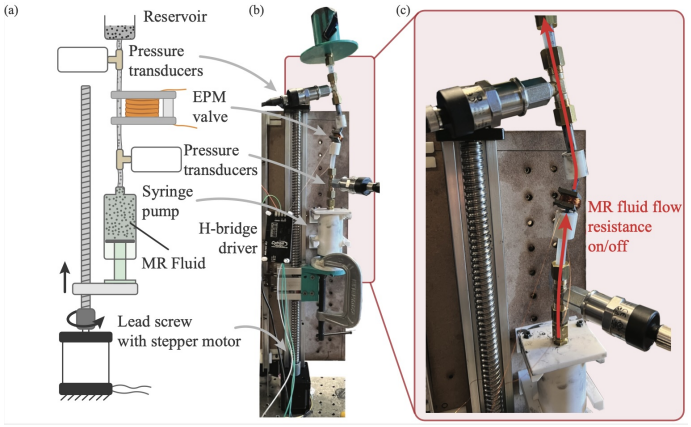

FIGURE 6: (A) SCHEMATIC DIAGRAM OF EXPERIMENTAL SETUP. (B) FULL VIEW OF CONSTRUCTED SETUP, (C) ENLARGED VIEW OF PUMP-VALVE CONFIGURATION

To isolate pressure due to the EPM valve closing or magnetic flux leakage from pressure caused by the setup (Syringe, MR fluid, flow-restriction), calibration tests were ran whereby the setup was actuated while filled with MR fluid, but without an EPM valve present. Subsequently, the setup was ran with valves mounted between the pressure transducers. The syringe was allowed to empty for some volume of liquid, establishing steady-state conditions with the valve open. Once this condition was met, a pulse of current was run through the solenoid to close the valve and steady state was allowed to form.

5. EXPERIMENTAL RESULTS

The results of running the test setup without an EPM valve attached to the flow restriction can be seen in Figure 7. Tests without the valve present demonstrated a baseline pressure difference of approximately 1 kPa caused by the viscosity of the MR fluid flowing through the narrow tube which acted as a flow restriction.

The first valve was tested to establish the functionality of the setup as it was a design known to work from the literature. The results of this test can be seen in Figure 8. During the test, the EPM valve was closed using a 200 ms pulse. After the pulse, the pressure across the valve increased from 1 kPa to 4.5 kPa.

The second valve, owing to its larger magnets, was expected to act as a larger flow restriction. From Figures 9 and 10 it can be seen that there may be flux leakage from this valve into the MR fluid as the initial steady-state pressure is higher than that of Figures 7 and 8. While the solenoid is turned on, there is a large spike in the effective resistance of the valve, shown in Figure 9 which settles back to approximately 2 kPa, demonstrating a failure of the valve to latch closed. Figure 10 demonstrates the valve which starts incompletely closed, evidenced by the high initial

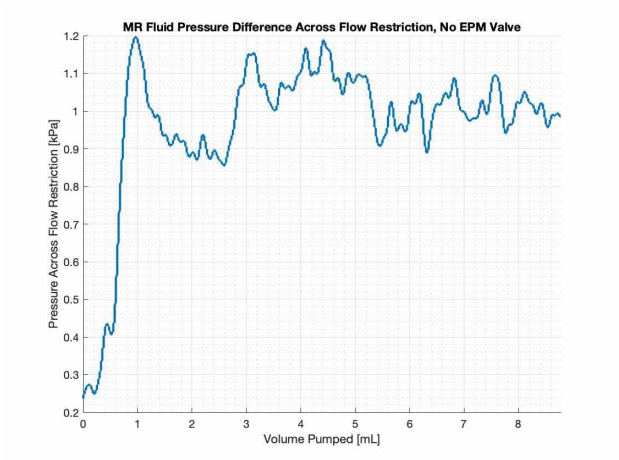

FIGURE 7: NOMINAL FLOW RESTRICTION OF THE SETUP WITHOUT THE EPM VALVE. FIGURE SHOWS THE PRESSURE DROP BETWEEN THE INLET AND OUTLET AT A CONSTANT FLOWRATE OF 0.625 mL/s.

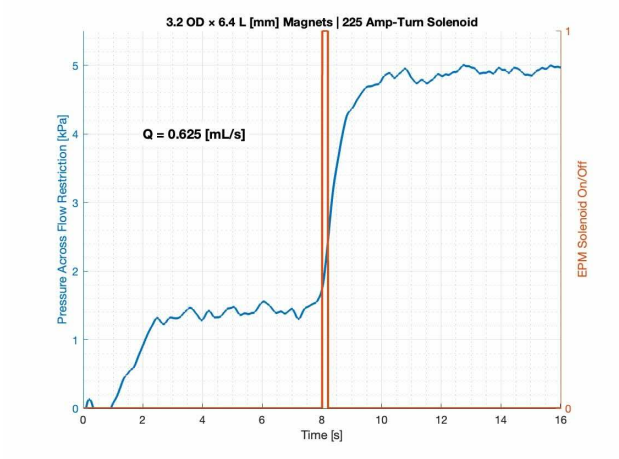

FIGURE 8: DEMONSTRATION OF THE EPM VALVE SHOWN IN FIGURE 5(A). THERE IS CLEAR DIFFERENTIATION BETWEEN THE VALVE OPEN AND CLOSED RESISTANCE.

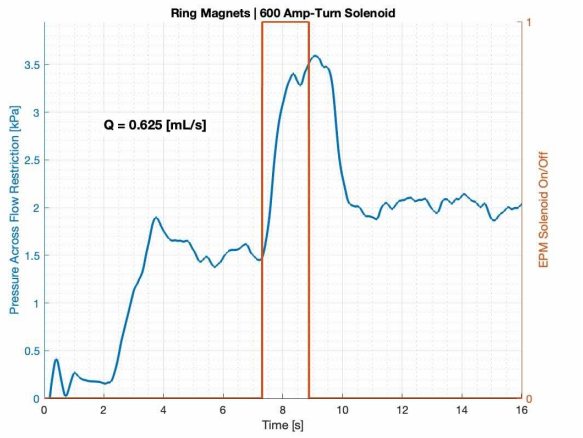

FIGURE 9: RESULTS OF TEST INVOLVING VALVE SHOWN IN FIGURE 5(B). 12.9 OD X 7.5 ID X 5.9 L MM AINICO | 6.4 OD X 3.2 ID X 6.4 L MM NDFEB. AN INITIAL SPIKE IN THE VALVE RESISTANCE IS CAUSED BY THE EXTENDED ENERGIZATION OF THE SOLENOID. HOWEVER, THE VALVE FAILED TO CLOSE.

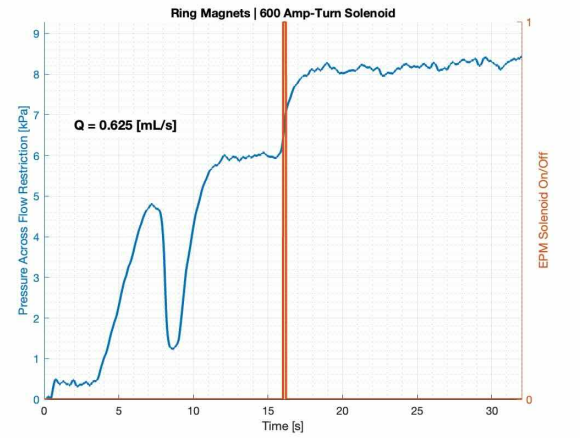

FIGURE 10: VALVE PRESENTED IN FIGURE 5(B). 12.9 OD X 7.5 ID X 5.9 L MM AINICO | 6.4 OD X 3.2 ID X 6.4 L MM NDFEB. INCOMPLETE OPENING OF THE VALVE CAUSED A HIGHER INITIAL FLOW RESISTANCE.

pressure prior to the electric pulse, but which is closed more completely by the pulse of current. While both Figures 9 and 10 demonstrate a failure of the valve to switch its configuration, they do give a baseline for the pressure differences which may be expected from the proposed EPM valve.

The results of the test using the proposed valve design can be seen in Figure 11. The initial resistance of the system at steady-state is higher than that of Figures 7 and 8. This may be due to flux leakage from the valve into the MR fluid, causing an increase in fluid viscosity. Similar to the results shown in Figure 9, the resistance of the valve only markedly increased while the solenoid was energized.

6. DISCUSSION

To enable a prime mover architecture for soft robotics, it will be necessary to develop compact valves which are capable of rapid actuation. Preferably, these valves would act as large resistances and be able to switch hydraulic loads at relatively high pressures. The proposed design is compact and easily manufactured. It is theoretically capable of switching on and off on a millisecond time-scale although that was neither investigated nor demonstrated for this work.

The exploratory prototype failed to toggle decisively on or off. There are potential issues with its construction that bear further investigation. For example, the exploratory prototype was constructed using readily-available magnets which were not ideally sized. It is possible that each magnet failed to provide an adequate return path for the flux provided by the other. The prototype used an AlNiCo magnet with much more magnetic material than the NdFeB magnet paired with it. This may have lead to flux leaking around the NdFeB magnet and into the MR fluid.

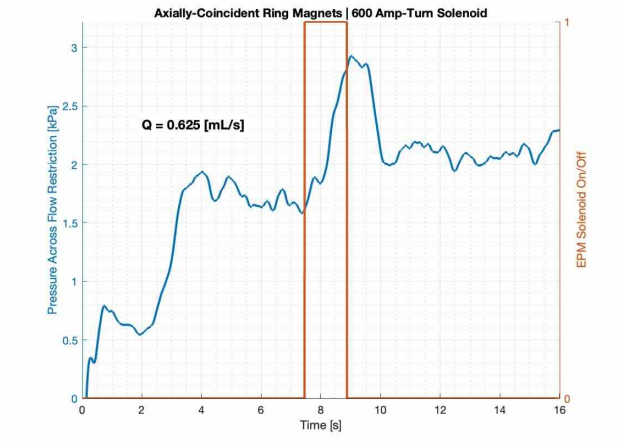

FIGURE 11: RESULTS OF TEST INVOLVING PROPOSED VALVE DESIGN. THERE IS AN INITIAL SPIKE IN VALVE RESISTANCE CAUSED BY THE EXTENDED ENERGIZATION OF THE SOLENOID. HOWEVER, THE VALVE EITHER FAILS TO CLOSE OR FAILS TO PROVIDE MEANINGFUL RESISTANCE.

The inability to toggle may also indicate a potential problem with re-magnetization of the AlNiCo magnet. It will be necessary to determine the conditions which will guarantee re-magnetization of the AlNiCo magnet such that the EPM can be turned "On" or "Off". A potential factor affecting AlNiCo re-magnetization is the NdFeB magnet within the solenoid coil. This magnet may disrupt the magnetic field generated by the solenoid, preventing full re-magnetization of the AlNiCo ring. A potential fix would be to invert the design such that a NdFeB ring magnet would fully envelop a core composed an AlNiCo ring magnet wrapped in a solenoid.

A more formal design investigation is necessary to explore factors salient to the design of these valves. To delve deeper into the design, a multi-physics simulation package (COMSOL) was employed to evaluate various design geometries and sizing options.

7. MULTI-PHYSICS DESIGN INVESTIGATION

7.1 Magnet Size Ratio

Each of the second two valves, B and C, used identical magnets and solenoids to each other; the only difference was their arrangement and the size of the ferrous flux return paths. It was expected that both of these valves, due to their larger magnets, would act as increased flow resistances while closed when compared to the smaller first valve, A. In both cases, the resistance of the physical valve in the open configuration was higher than that of the system with no valve. This may be due to incompatible magnet sizes causing an increase in flux leakage into the MR fluid. The annular surface area of the AlNiCo magnet in contact with the iron flux directing end-cap was 87.7 mm^2 while that of the NdFeB ring was 24.1 mm^2. This means that the AlNiCo magnet is approximately 3.6× the area and volume of the NdFeB magnet which may lead to inadequate flux return and increased flux leakage into the MR fluid. For this reason, a simulation was conducted using magnets of identical cross-sectional area and length.

Figure 12 shows the results of the simulation conducted using magnets of equal cross-sectional area. The results support the notion that the different sizes of the magnets used may create an imperfect flux return, causing excessive leakage into the MR fluid and preventing the valve from ever attaining its most open configuration. In particular, the average flux density norm in the MR fluid of the nominal design, shown in Figure 12a in the "Open" state was found to be 0.61 T, approximately 10× higher than the corresponding predicted flux density norm of 0.06 T with equally sized magnets as shown in Figure 12b. These results suggest that by using magnets with appropriate size ratios, the performance of the valve in the open configuration may be increased. This adds a point of difficulty into the design of these valves whereby it may be difficult to source compatible magnets.

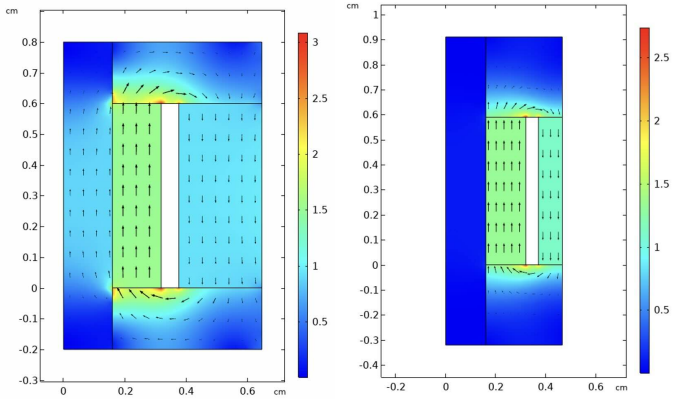

(a) EPM valve in open state with magnets used in experiment. **(b) EPM valve in open state with equal-area magnets**

FIGURE 12: COMSOL SIMULATION OF EPM VALVE USING DIFFERENT MAGNET RATIOS. A: NOMINALLY-SIZED RING MAGNETS. B: EQUIVALENTLY-SIZED RING MAGNETS. COLOR SCALE IN TESLA

7.2 Flux Concentration

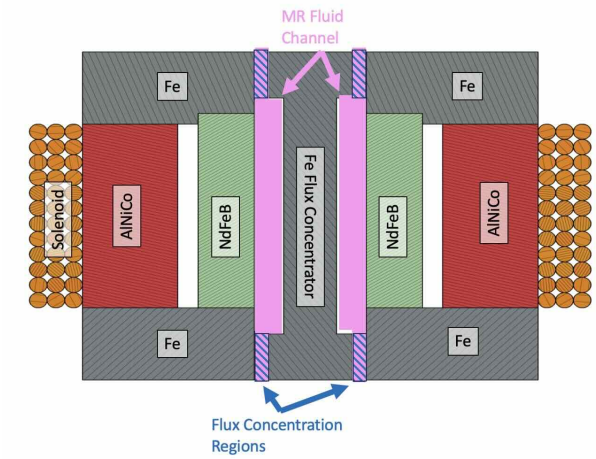

FIGURE 13: CROSS-SECTION OF PROPOSED VALVE WITH FLUX-CONECTRATING CORE. BLUE: REGIONS OF INCREASED FLUX DENSITY.

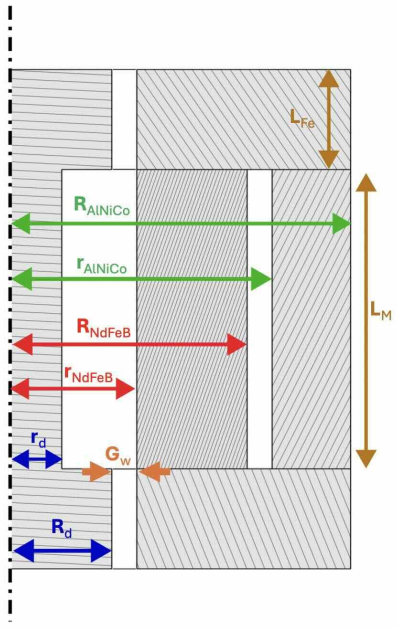

FIGURE 14: QUARTER-VIEW OF PROPOSED VALVE WITH NAMED DIMENSIONS GIVEN IN TABLE 1

TABLE 1: DIMENSIONS USED IN SIMULATIONS EXAMINING EFFECT OF FLUX CONCENTRATION CORE GAP WIDTH G_w ON EPM VALVE FLOW RESTRICTION AS SIMULATED IN FIGURE 15. ALL DIMENSIONS IN MM

Dimension	G_w =N/A	$G_w = 0.5$
r_d	N/A	1.00
R_d	N/A	2.00
r_{NdFeB}	1.50	2.50
R_{NdFeB}	4.26	4.71
r_{AlNiCo}	4.76	5.21
R_{AlNiCo}	6.44	6.78
L_M	6.00	6.00
L_{Fe}	2.00	2.00

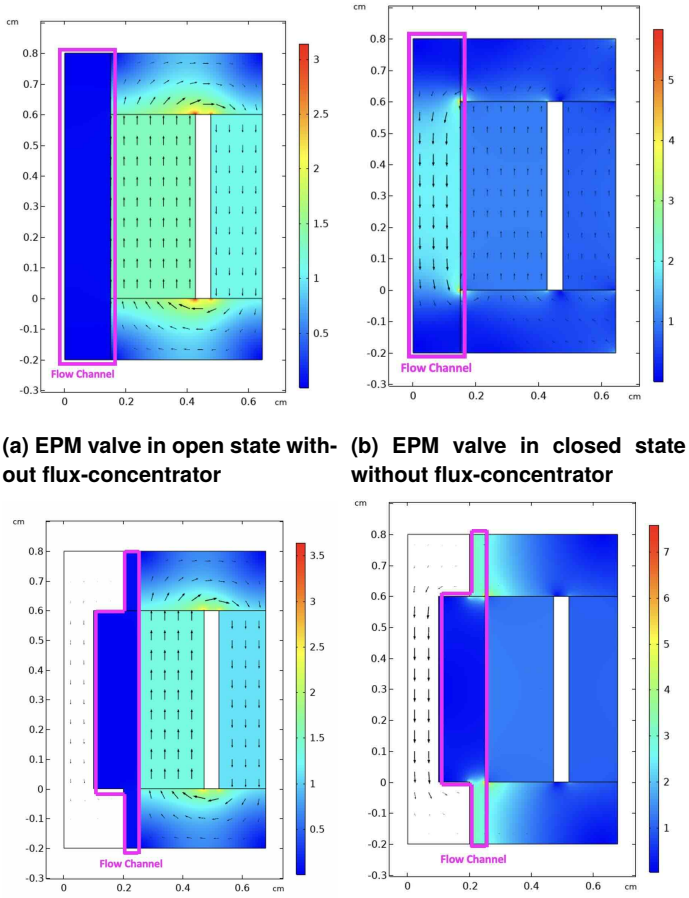

(a) EPM valve in open state without flux-concentrator

(b) EPM valve in closed state without flux-concentrator

(c) EPM valve in open state without flux-concentrator

(d) EPM valve in closed state with flux-concentrator

FIGURE 15: COMSOL SIMULATION OF EPM VALVE (A) WITHOUT FLUX-CONCENTRATOR, OPEN (B) WITHOUT FLUX-CONCENTRATOR, CLOSED (C) WITH FLUX-CONCENTRATOR, OPEN (D) WITH FLUX-CONCENTRATOR, CLOSED. COLOR SCALE HAS UNITS OF TESLA. COLOR SCALE TURNED OFF IN FLUX-CONCENTRATOR FOR CLARITY OF SCALE.

Simulations were run to determine the effects of including a flux-concentrating core (Figure 13) which creates a constant-width annulus within the valve's bore using the dimensions specified by Figure 14 and Table 1 on the change in fluid resistance between the open and closed valve configurations. These dimensional values make it so that for each simulation, the amount of magnetic material is constant and related by the ratio $A_{NdFeB} : A_{AlNiCo} = B_{r-NdFeB} : B_{r-AlNiCo}$ where A_i is the cross-sectional area of the ring magnet and B_{r-} is the remanent flux density of the respective magnetic material ($B_{r-NdFeB}$ = 1.3 T,$B_{r-AlNiCo}$ = 1.1 T). This should, in theory mitigate the flux leakage from the EPM into the MR fluid. These values also make it so that the annulus caused by the core has equal area to the nominal hole without the flux-concentrating core.

Figure 15 shows plots of simulations using the proposed design with (Figures 15c and 15d) and without (Figures 15a and 15b) the addition of a ferrous insert to concentrate flux as in Figure 13. For each of these simulations, a pressure difference of 68.95 kPa was applied across the valve.

Table 2 shows the values of flow and resistance achieved by the simulated valve without and with the inclusion of the flux-concentrating core when a pressure difference of 68.95 kPa is applied across the valve. A fully-developed laminar flow model was used within COMSOL to calculate the mass flow rate through the valve. Fluid friction is ignored.

These results show that the inclusion of the dumbbell-shaped flux-concentrator is associated with an increase in the average flux density in the MR fluid (1.30 to 3.032 T) when the valve is in the closed configuration. However, it is also associated with an increase in the average flux density through the MR fluid in the open configuration (0.025 to 0.058 T). In the closed configuration, the valve with the concentrator permitted less fluid flow, however, it also permitted less flow while open than did the valve simulated without the flux-concentrator.

The valve with the flux-concentrator showed a higher ratio of resistance between its open and closed configurations which is

TABLE 2: RESULTS OF SIMULATION SHOWN IN FIGURE 15

Nominal	Closed	Open	Closed/Open
$\bar{B}$ (T)	1.30	0.025	52
Q (mL/s)	1.423	52.333	0.027
$R = P/Q$ (Pa s/m^3)	$4.84x10^{10}$	$1.315x10^{9}$	37
Flux-concentrator	Closed	Open	Closed/Open
$\bar{B}$ (T)	3.032	0.058	52
Q (mL/s)	0.106	4.867	0.0217
$R = P/Q$ (Pa s/m^3)	$6.516x10^{11}$	$1.418x10^{10}$	46

an encouraging development for further investigation. The power dissipated in the valve ($P = Q^2R$, where P is power in Watts) while open was calculated. This showed a 3.6 W dissipation by the valve without the flux-concentrator but a 0.34 W dissipation by the valve with the flux-concentrator when subject to a pressure difference of 68.95 kPa across the valve in the open configuration. This is an important metric when considering the efficiency of a system that would use these valves.

The viscosity and rheological behavior of MR fluid is of particular note when it is desired for use as a hydraulic working fluid and controlled using EPM valves. MR fluid jams and solidifies in the presence of magnetic fields, behaving like a Bingham plastic [4]. Stronger magnetic fields are able to better solidify the fluid. One limitation of this study is that MR fluid was considered as a variable-viscosity fluid rather than a Bingham plastic. Therefore, rigid body behavior is expected at high magnetic flux densities and viscous fluid behavior at either low magnetic flux densities or sufficient stress. This is not captured in the present simulations. Given MR fluid behaving as a Bingham plastic, we would expect to see higher resistance values for the configuration with the flux concentrator due to both its increased flux density and its higher overall resistance.

8. CONCLUSIONS

EPM valves show potential for the control of fluid flow in soft robotics. They consume no power except when changing between their open and closed states. Additionally, they have no moving parts, can be made compact, and feature rapid switching times. In this work, a new design for an EPM valve was proposed and tested both in simulation and experimentally. The physical implementation was unable to achieve meaningful flow resistance, and in particular, failed to latch into the open or closed configurations. For this reason, a design study was conducted leveraging multi-physics simulation to explore the factors which influence the performance of the valve. From these simulations, different design criteria were explored which will enable the creation of EPM valves with lower flow resistances while in their open configurations and higher flow resistances while in their closed configurations.

The multi-physics simulation study indicated that performance of the exploratory valve in its open configuration may have been limited by incorrect sizing of the magnets used. It was found via simulation that the magnetic materials used must have compatible sizes relative to each other to mitigate flux leakage into the MR fluid. Using properly sized magnets will allow the valve a lower fluid resistance in the open configuration. Simulation suggested that the magnets should possess cross-sectional areas which are scaled to each magnetic material's remanent flux density.

The simulations also indicated that the inclusion of a flux-concentrating core made from ferrous material has the effect of drastically increasing the magnetic flux density in selected active regions of the fluid channel of the valve.

The proposed design is relatively simple and easy to manufacture. It enables the use of a larger magnet-to-volume ratio within the EPM valve and simplifies inclusion of the EPM solenoid. With the potential increase in the valve's closed configuration fluid resistance from using a flux concentrator and decrease in the valve's open configuration resistance by careful magnet selection, it is likely that the proposed design will be able to function in a manner which brings the proposed soft robotic prime mover architecture closer to reality.

9. ACKNOWLEDGMENT

This work was funded by the National Science Foundation Expanding Frontiers in Research and Innovation Program, grant number 1935278.

REFERENCES

[1] Kennedy, Buresch K. C. Boinapallay P. et al., E. B. L. "Octopus arms exhibit exceptional flexibility." *Sci Rep* Vol. 10 No. 20872 (2020).

[2] (2023). URL https://bostondynamics.com/atlas/.

[3] Böse, Holger, Rabindranath, Raman and Ehrlich, Johannes. "Soft magnetorheological elastomers as new actuators for valves." *Journal of Intelligent Material Systems and Structures* Vol. 23 No. 9 (2012): pp. 989–994. DOI 10.1177/1045389X11433498. URL https://doi.org/10.1177/1045389X11433498, URL https://doi.org/10.1177/1045389X11433498.

[4] McDonald, Kevin J., Kinnicutt, Lorenzo, Moran, Anna Maria and Ranzani, Tommaso. "Modulation of Magnetorheological Fluid Flow in Soft Robots Using Electropermanent Magnets." *IEEE Robotics and Automation Letters* Vol. 7 No. 2 (2022): pp. 3914–3921. DOI 10.1109/LRA.2022.3147873. Accessed 2024-03-26, URL https://ieeexplore.ieee.org/document/9699046. Conference Name: IEEE Robotics and Automation Letters.

[5] Ntella, Sofia Lydia, Thabuis, Adrien, Tiwari, Bhawnath, Jeanmonod, Kenny, Koechli, Christian and Perriard, Yves. "Highly Efficient Miniaturized Magnetorheological Valves Using Electropermanent Magnets." *IEEE Robotics and Automation Letters* Vol. 8 No. 3 (2023): pp. 1487–1494. DOI 10.1109/LRA.2023.3238669. Accessed 2024-03-27, URL https://ieeexplore.ieee.org/document/10023972/.

[6] Leps, T., Glick, P. E., III, D. Ruffatto, Parness, A., Tolley, M. T. and Hartzell, C. "A low-power, jamming, magnetorheological valve using electropermanent magnets suitable for distributed control in soft robots." *Smart Materials and Structures* Vol. 29 No. 10 (2020): p. 105025. DOI 10.1088/1361-665X/abadd4. Accessed 2024-03-27, URL

https://dx.doi.org/10.1088/1361-665X/abadd4. Publisher: IOP Publishing.

[7] McDonald, Kevin, Rendos, Abigail, Woodman, Stephanie, Brown, Keith A. and Ranzani, Tommaso. "Magnetorheological Fluid-Based Flow Control for Soft Robots." *Advanced Intelligent Systems* Vol. 2 No. 11 (2020): p. 2000139. DOI https://doi.org/10.1002/aisy.202000139. URL https://onlinelibrary.wiley.com/doi/pdf/10.1002/aisy.202000139, URL https://onlinelibrary.wiley.com/doi/abs/10.1002/aisy.202000139.

[8] Gallentine, James and Barth, Eric J. "3D Printed Gerotor Pump Geometries for Soft-Robot Actuation." 2023. American Society of Mechanical Engineers Digital Collection. DOI 10.1115/FPMC2023-111408. Accessed 2024-03-27, URL https://dx.doi.org/10.1115/FPMC2023-111408.

[9] Lo Sciuto, Grazia, Kowol, Paweł and Pilśniak, Adam. "Automated measurements and characterization of magnetic permeability in magnetorheological fluid." *Microfluidics and Nanofluidics* Vol. 26 No. 8 (2022). URL http://proxy.library.vanderbilt.edu/login?url=https://www.proquest.com/scholarly-journals/automated-measurements-characterization-magnetic/docview/2684783298/se-2. Copyright - © The Author(s), under exclusive licence to Springer-Verlag GmbH Germany, part of Springer Nature 2022; Last updated - 2023-11-29.

[10] Orsavova, Jana, Misurcova, Ladislava, Vavra Ambrozova, Jarmila, Vicha, Robert and Mlcek, Jiri. "Fatty Acids Composition of Vegetable Oils and Its Contribution to Dietary Energy Intake and Dependence of Cardiovascular Mortality on Dietary Intake of Fatty Acids." *International Journal of Molecular Sciences* Vol. 16 No. 6 (2015): pp. 12871–12890. DOI 10.3390/ijms160612871. Accessed 2024-03-27, URL https://www.ncbi.nlm.nih.gov/pmc/articles/PMC4490476/.

[11] Jinaga, Rakesh, Jagadeesha, T., Kolekar, Shreedhar and Choi, Seung-Bok. "The Synthesis of Organic Oils Blended Magnetorheological Fluids with the Field-Dependent Material Characterization." *International Journal of Molecular Sciences* Vol. 20 No. 22 (2019): p. 5766. DOI 10.3390/ijms20225766. Accessed 2024-03-27, URL https://www.ncbi.nlm.nih.gov/pmc/articles/PMC6888077/.